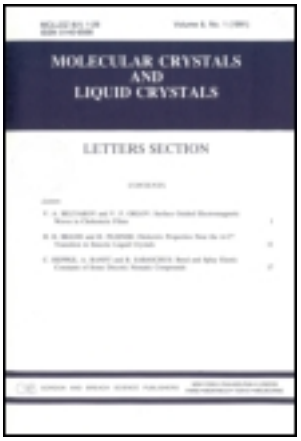

Molecular Crystals and Liquid Crystals
Publication details, including instructions for authors and subscription information:
http://www.tandfonline.com/loi/gmcl20

Effects of Charge Balance on the Carrier Trapping Mechanisms of Organic Light-Emitting Devices with a 5,6,11,12-Tetraphenylnaphthacene Emission Layer

Jae Seung Jang [a] , Su Hyeong Park [b] , Dae Hun Kim [b] & Tae Whan Kim [a b]

[a] Department of Information Display Engineering , Hanyang University , Seoul , 133-791 , Korea
[b] Department of Electronics and Computer Engineering , Hanyang University , Seoul , 133-791 , Korea
Published online: 16 Dec 2013.

To cite this article: Jae Seung Jang , Su Hyeong Park , Dae Hun Kim & Tae Whan Kim (2013) Effects of Charge Balance on the Carrier Trapping Mechanisms of Organic Light-Emitting Devices with a 5,6,11,12-Tetraphenylnaphthacene Emission Layer, Molecular Crystals and Liquid Crystals, 583:1, 159-169, DOI: 10.1080/15421406.2013.844382

To link to this article: http://dx.doi.org/10.1080/15421406.2013.844382

Mol. Cryst. Liq. Cryst., Vol. 583: pp. 159–169, 2013

ISSN: 1542-1406 print/1563-5287 online
DOI: 10.1080/15421406.2013.844382

Taylor & Francis
Taylor & Francis Group

Effects of Charge Balance on the Carrier Trapping Mechanisms of Organic Light-Emitting Devices with a 5,6,11,12-Tetraphenylnaphthacene Emission Layer

JAE SEUNG JANG,[1] SU HYEONG PARK,[2] DAE HUN KIM,[2] AND TAE WHAN KIM[1,2,*]

[1]Department of Information Display Engineering, Hanyang University, Seoul 133-791, Korea
[2]Department of Electronics and Computer Engineering, Hanyang University, Seoul 133-791, Korea

The efficiency of the organic light-emitting devices (OLEDs) was enhanced with increasing thickness of a 5,6,11,12-tetraphenylnaphthacene (rubrene) emission layer (EML). The charge trapping and the luminance mechanisms were affected by the thickness of the rubrene layer, regardless of the existence of the barrier layers. The variation in the electroluminescence spectra of devices originated from a variation in the position of the recombination region with increasing thickness of the EML. The enhancement of the luminescence efficiency for devices was attributed to the better charge balance and the optimized recombination region.

Keywords Carrier trapping mechanisms; charge balance; electrical property; OLEDs; optical property; rubrene EML

PACS numbers 85. 60 Jb; 68. 37. Hk; 78. 60. Fi

Introduction

Organic light-emitting devices (OLEDs) have emerged as potential candidates for applications in promising next-generation full-color display systems and light sources due to their excellent advantages of high contrast, fast response, thin thickness, light weight, and low power consumption [1–5]. The prospect of potential applications of OLEDs in display systems has led to substantial research and development efforts to enhance their luminance efficiency [6–10]. However, the device performances of OLEDs still have inherent problems for potential applications in commercial products due to their low efficiency, short lifetime, and poor stability [11–13]. Doping with various dopant materials in the host materials of the OLEDs have been suggested to improve their luminance efficiency [14,15], and OLEDs with a 5,6,11,12-tetraphenylnaphthacene (rubrene)-doped emission layer (EML) have drawn a great deal of interest because of their high efficiency [16]. Because the carrier

*Address correspondence to Prof. Tae Whan Kim, Department of Electronics and Computer Engineering, Hanyang University, 222 Wangsimni-ro, Seongdong-gu, Seoul 133-791, Korea (ROK). Tel.: (+82)02-2220-0354; Fax: (+82)02-2292-4135. E-mail: twk@hanyang.ac.kr

trapping behaviors in the rurbrene layer reduce the efficiency of the rubrene-doped EML, studies on the carrier trapping mechanisms of OLEDs with a rubrene EML are necessary to enhance their luminance efficiency [17]. Even though some studies on the electrical and the optical properties of OLEDs with a rubrene-doped EML have been performed, very few investigations on the effects of carrier balance on the carrier trapping mechanisms in OLEDs with a rubrene EML have been clarified. Furthermore, systematic studies on the effects of carrier balance on the carrier trapping mechanisms in OLEDs are necessary to enhance device efficiency.

This paper reports data for the charge balance effects on the carrier trapping mechanisms in OLEDs with a rubrene EML. Current density-voltage, luminance-voltage, electroluminescence (EL) spectra measurements for the OLEDs with a rubrene EML were performed to investigate their charge trapping and luminance mechanisms. The carrier trapping mechanisms of the OLEDs with a rubrene EML were described on the basis of their experimental results.

Experimental Details

The sheet resistance and the thickness of the indium-tin-oxide (ITO) substrates used in this study were 15 Ω/square and 150 nm, respectively. The ITO substrates were cleaned in trichloroethylene, acetone, and methanol sequentially at 60°C for 15 min by using an ultrasonic cleaner and were rinsed thoroughly in de-ionized water. After the chemical cleaning, the ITO substrates were dried by using N_2 gas with a purity of 99.9999%, and the surfaces of the ITO substrates were treated with an ultraviolet-ozone cleaner for 10 min at room temperature at a system pressure of 1 atm. After the cleaned ITO substrates had been loaded into the evaporation chamber to fabricate the devices, the organic layers and the metal cathode layer were deposited on the ITO substrates at a system pressure of 6×10^{-7} Torr. The OLEDs utilizing various kinds of EMLs were fabricated with the following structures from the top: an Al cathode/a lithium quinolate (Liq) electron injection layer (EIL)/a tris (8-hydroxyquinoline) aluminum (Alq_3) electron transport layer (ETL)/a 2,9-dimethyl-4,7-diphenyl-1,10-phenanthroline (BCP) hole blocking layer (HBL)/various kinds of EMLs/an N,N-bis-(1-naphthyl)-N,N-diphenyl-1,1-biphenyl-4,4-diamine (NPB) hole transport layer (HTL)/an ITO-coated glass substrate. Schematic diagrams of devices I, II, III, IV, and V are shown in Fig. 1.

The undoped rubrene EML and the BCP layer were typically deposited with a thickness of 10 nm to investigate the changes in the electrical and the optical properties due to variations in the charge balances in devices I and II. While the thicknesses of the NPB and the Alq_3 layers were changed, the total thickness of the NPB and the Alq_3 layers was fixed at 80 nm. The thickness of the Alq_3 layer for devices I and III was 40 nm, and that for devices II, IV, and V was 30 nm. The thickness of the rubrene EML for devices I and II was 10 nm, and that for devices III, IV, and V was 30 nm. An Al cathode with a thickness of 100 nm was deposited on the active layer by using thermal evaporation. The growth rates of the organic layers and the metal layers were approximately 0.5 and 1 Å/s, respectively, which were controlled by using a quartz-crystal deposition rate/thickness monitor (Sigma, SQM-160). The emitting pixel area of the rubrene devices was 2×2 mm^2.

The current-voltage characteristics were measured on a programmable electrometer with a built-in current and voltage measurement system (M6100, McScience). The brightness was measured by using a brightness meter, and the EL spectrum was measured by using a luminescence spectrometer (CS-1000, Minolta) with a voltage step appliance.

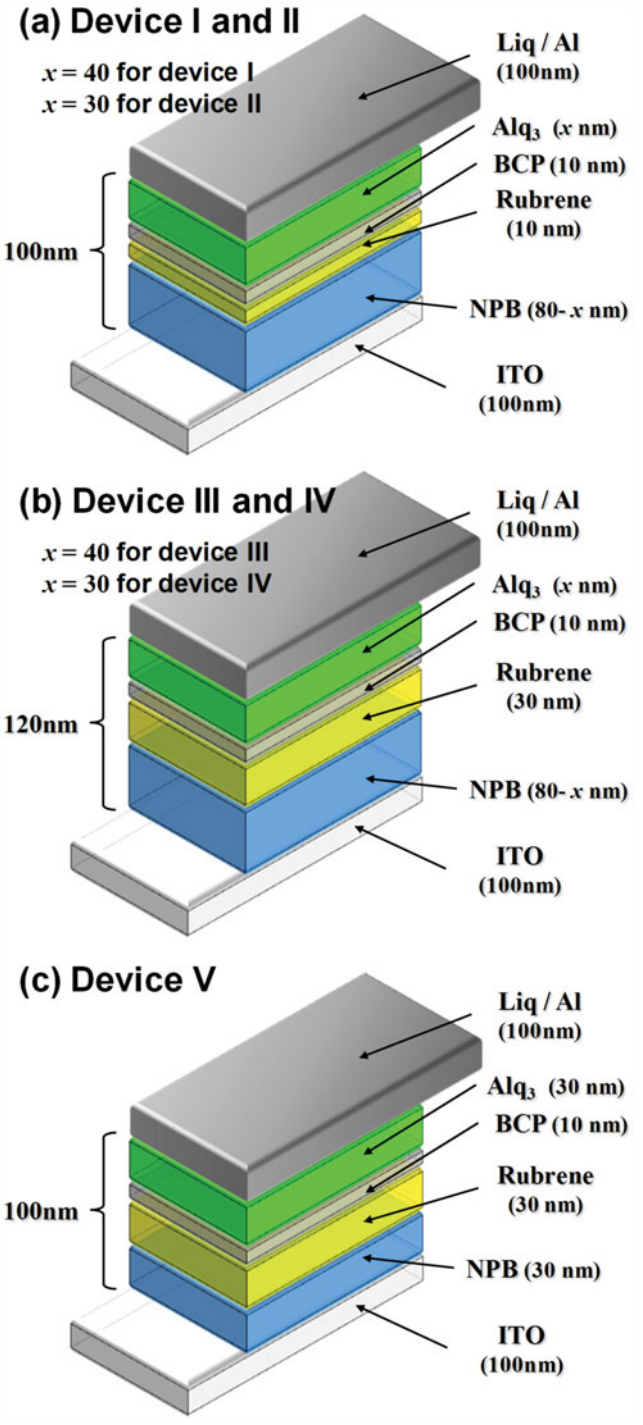

Figure 1. Schematic diagrams of devices I, II, III, IV, and V.

Results and Discussion

The energy band diagrams of devices I, II, III, IV, and V are shown in Fig. 2. Because the highest occupied molecular orbital (HOMO) level of the rubrene is higher than that of the NPB hole transport layer (HTL) and the HOMO level of the BCP hole blocking layer (HBL) is much lower than that of the rubrene, the holes existing in the NPB HTL are efficiently injected from the NPB layer to the rubrene layer. The holes are effectively blocked at the rubrene/BCP heterointerface due to the high barrier height of the HOMO energy level. The lowest unoccupied molecular orbital (LUMO) level of the rubrene layer is slightly larger than that of the BCP layer and much lower than that of the NPB HTL layer. While the electrons are effectively injected from the Alq_3 electron transport layer (ETL) into the BCP layer [18], they are blocked by the high energy barrier height at the rubrene/NPB heterointerface. Therefore, the electrons and the holes injected into the rubrene EML are negligible due to the high energy barrier, and the charge balance in the rubrene is dominantly affected by the hole mobility of the NPB layer and the electron mobility of the Alq_3 layer. Thus, the carrier-balance variation in the EML can be achieved by controlling the thicknesses of the NPB HTL and the Alq_3 ETL in OLEDs while keeping the thicknesses of the rubrene EML and the BCP HBL constant. The thickness of the rubrene EML for devices I and II was 10 nm, and that for devices III, IV, and V was 30 nm. While the thickness of the Alq_3 layer for devices I and III was 40 nm and that for devices II, IV, and V was 30 nm, the total thickness of the Alq_3 and the NPB layers was fixed at 80 nm. The performance characteristics of devices are compared by changing thickness of the rubrene EML and total thickness of devices.

Figure 3 shows the (a) current density-voltage (J-V), the (b) luminance-voltage, and the (c) luminance efficiency-current density characteristics of devices I, II, III, IV, and V. While the turn-on voltage of device II is the lowest among the devices, its brightness and luminance efficiency are the highest. The enhancement of the brightness and the luminance efficiency of device II is attributed to the optimum thicknesses of the NPB HTL and the Alq_3 ETL. Because the barrier height for carrier injection is negligible due to the small thickness of the rubrene EML, the charge balance of the electrons and the holes in the rubrene EML is dominantly affected by the carrier transport properties of the NPB and the Alq_3 layers. The turn-on voltage of device II is smaller than that of device I due to an increase in the electron current density resulting from the thinner Alq_3 layer. In addition, the recombination zone for excitons becomes closer to the Al electrode with decreasing thickness of the Alq_3 EML, the luminance of device II decreases.

Figure 3(c) shows the luminance efficiency-current density characteristics of devices I, II, III, IV, and V. The luminance efficiencies of devices II and IV with a optimum thickness of the Alq_3 layer at the same current density are higher than those of devices I, III, and V. The luminance efficiency of device II with an EML containing excess holes is similar to that of device I with an EML containing excess electrons. While the luminance efficiencies of devices I, II, and IV decrease with increasing current density, those of devices III and V remain constant, regardless of the current density. Because the thicknesses (10 nm) of the EMLs of devices I and II are smaller than the widths of their recombination region, resulting in the appearance of luminescence in the entire EML region, the recombination region does not shift, regardless of the current density. However, the thickness (30 nm) of the EMLs for devices III, IV, and V is larger than the width of their recombination regions, the position of the recombination region in the EML shifts with varying current density.

Figure 4 shows a log-log plot of the J-V characteristics of devices II and V. Figure 4 shows the fitted data for two current transport mechanisms in different voltage regions.

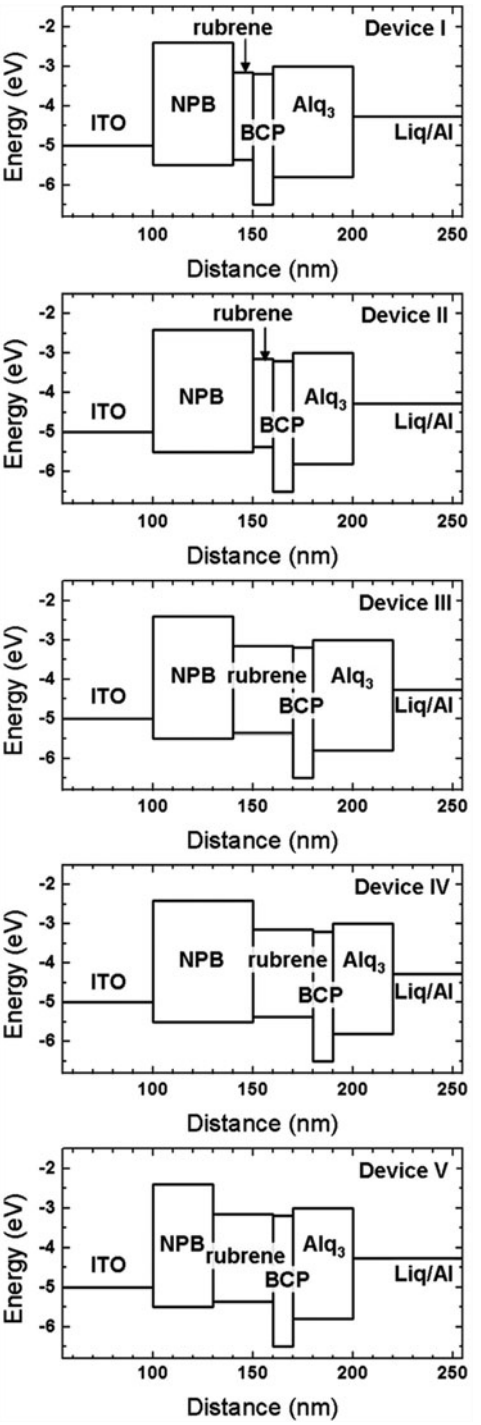

Figure 2. Schematic band diagrams of devices I, II, III, IV, and V.

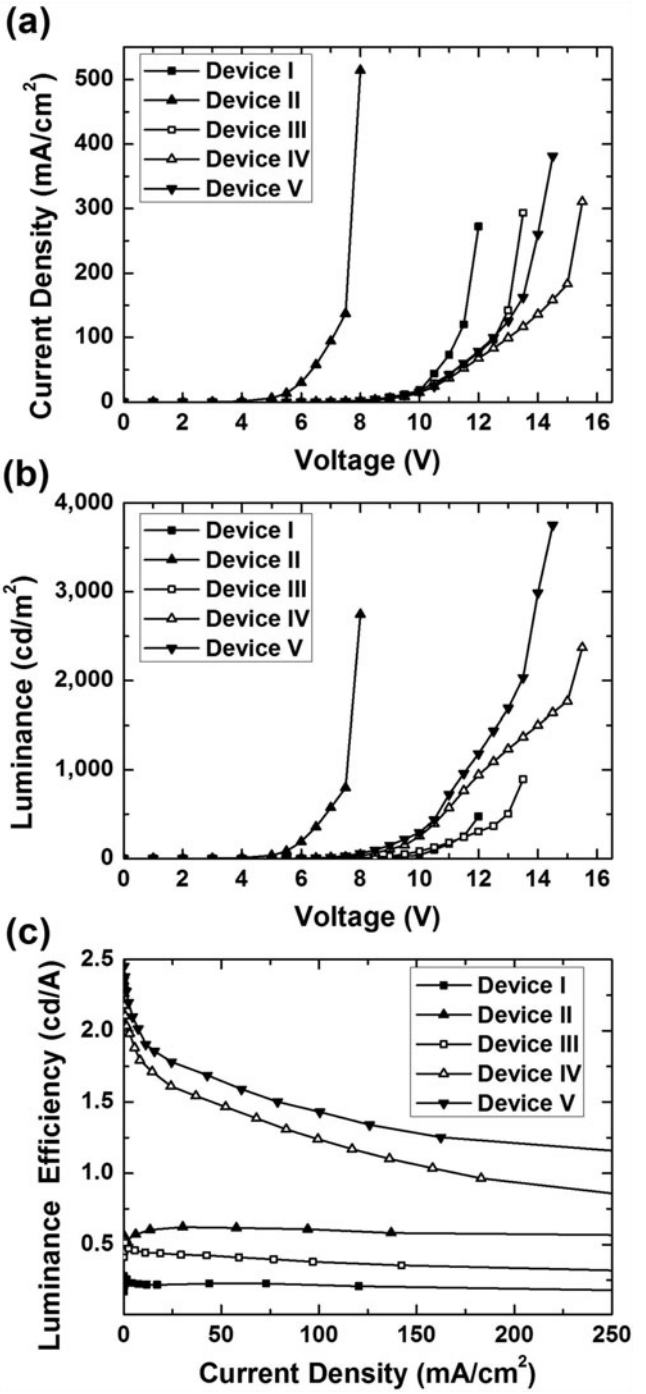

Figure 3. (a) current density-voltage, (b) luminance-voltage, and (c) current efficiency-current density characteristics of devices I, II, III, IV, and V.

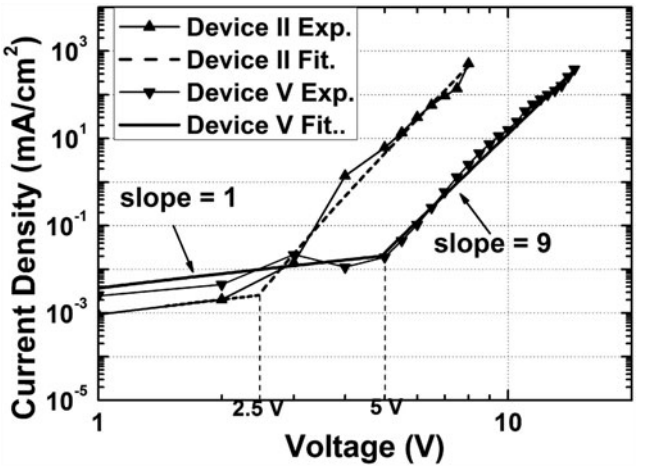

Figure 4. Log-log plot of the current density-voltage characteristics of devices II and V.

Because the measured currents with very small magnitudes did not show a reasonable dependence on the applied voltage [18], the fitted data for the J-V curves were not available over the entire applied voltage ranges. The J-V curves exhibit two regions with different slopes. The slope of the J-V curves below the transition voltage is 1, indicative of an Ohmic region. The data at lower voltages up to the transition voltage can be well fitted with an Ohmic current mechanism, where ln(J) is plotted against V, indicating that the electrical conduction is governed by Ohm's law in this range. The J-V characteristics above the transition voltage show a large linear slope of 9, which is the typical value of a trap-charge limited conduction mechanism. Therefore, even though the thickness of the rubrene EML for devices II an IV changes, while the turn-on voltage of the devices varies, the trap energy remains constant. The experimental J-V curves for devices II and V are in reasonable agreement with the simulation curves, as shown in Fig. 4.

Figure 5 shows the EL spectra of devices I, II, III, IV, and V at (a)100 mA/cm^2 and (b) 100 cd/m^2. A dominant main peak around 560 nm, together with a shoulder peak near 600 nm, appears to all devices with a rubrene EML. The variation in the EL spectra of the devices at the same current density is attributed to the magnitude of generated excitons being differed from that of injected carriers. The number of photons emitted in the EML is proportional to the magnitude of generated excitons, and the intensity of the shoulder peak for device with a high luminescence efficiency increases due to the enhancement of excitons at the same carrier injection, as shown in Fig. 5(a). The EL spectra related to the rubrene EML of devices at the same luminance do not change, regardless of the carrier balance. Because the thicknesses (10 nm) of the EMLs for devices I and II are very small, the positions of the recombination regions in the EMLs are the same, regardless of variations in the thicknesses of the NPB and the Alq_3 layers. The EL peaks related to the Alq_3 and the NPB layers of devices III and IV do not appear due to the perfect recombination of electron-hole pairs in the EML resulting from the large thickness of the EML. The intensity of the shoulder peak around 600 nm corresponding to the rubrene layer of devices III and IV varies with changing charge balance. The difference in the EL spectra of devices III and IV with a rubrene EML at the same current density is attributed to the different positions of the recombination regions and the different numbers of excitons generated in the EML. The variation in the EL spectra of devices III and IV is related to a variation in the position of the

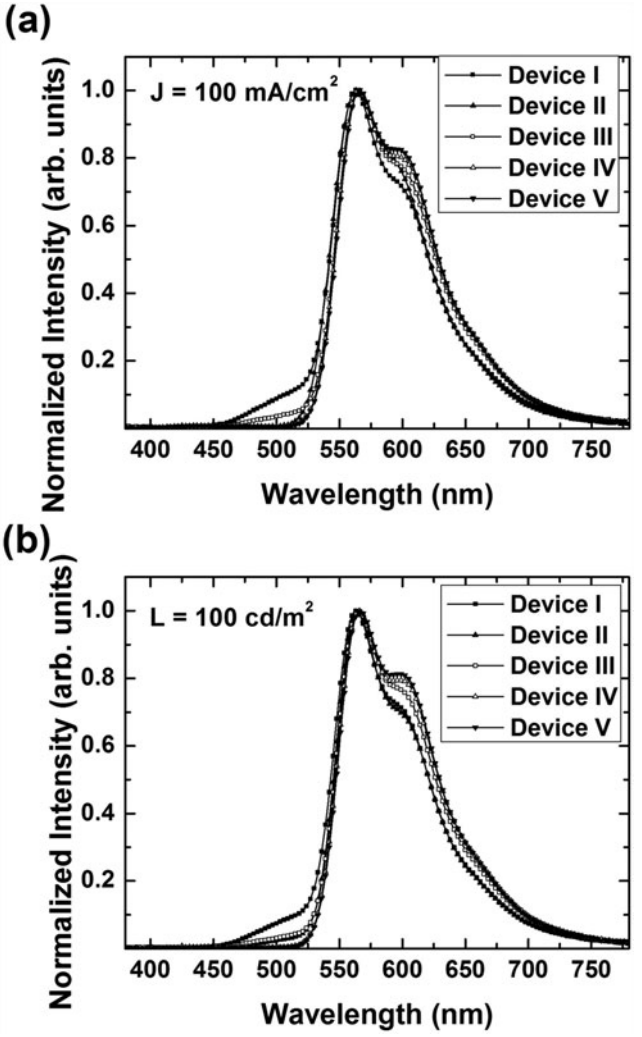

Figure 5. Electroluminescence spectra of devices I, II, III, IV, and V at (a) 100 mA/cm^2 and (b) 100 cd/m^2.

recombination region with increasing thickness of the EML. The improved luminescence efficiency for device IV in comparison with device III is attributed to a better charge balance and a larger recombination region.

Figure 6 shows multiple Gaussian spectral analyses of the EL spectra of devices (a) II, (b) IV, and (c) V at 100 cd/m^2. The positions of the analyzed Gaussian functions of the EL spectra for devices II, IV, and V are around 560, 600, and 630 nm, respectively. While the intensity and the full width at half maximum (FWHM) of the peak at 560 nm for device II are almost same as those of devices IV and V, the intensities of the peaks at 600 and 630 nm for device II are different from those values for the corresponding peaks for devices IV and V. Because the energy levels of the HOMO and the LUMO of the rubrene layer are -5.36 and -3.15 eV, respectively, the energy gap of the rubrene is 2.21 eV. The average wavelength of the main peak for device V with the strongest shoulder-peak intensity is

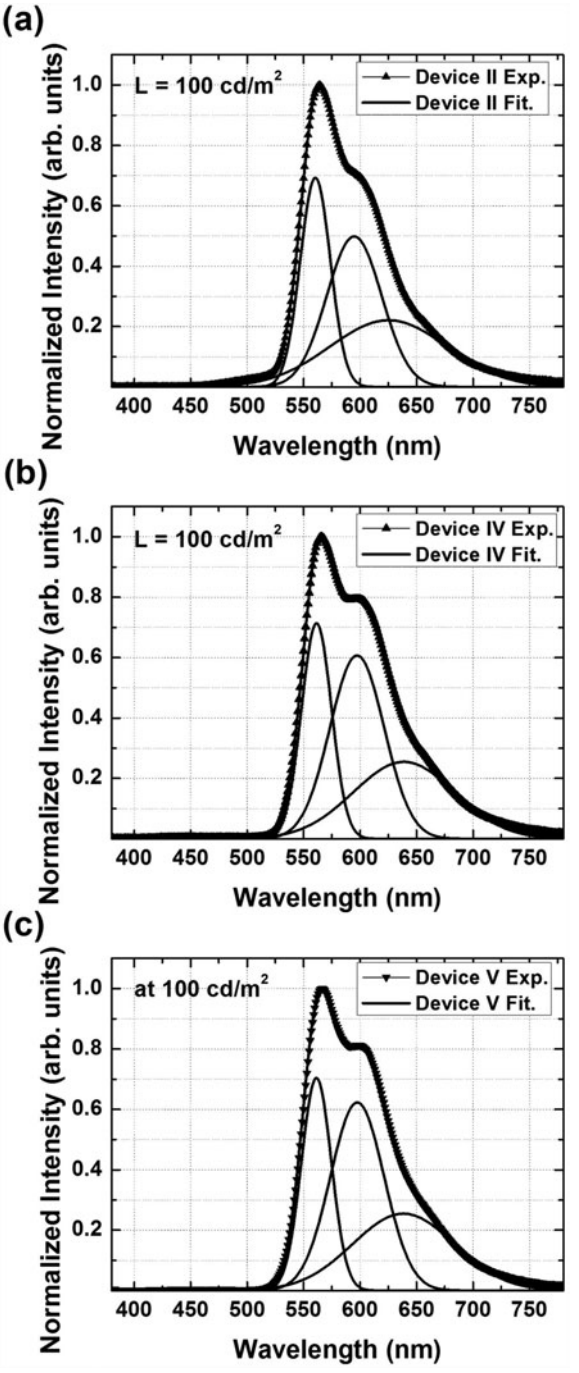

Figure 6. Multiple Gaussian spectral analyses of the EL spectra of devices (a) II, (b) IV, and (c) V at 100 cd/m^2.

561.39 nm (2.21 eV), which corresponds to the energy gap of the rubrene. The EL peaks at 597.56 (2.08 eV) and 638. 44 nm (1.94 eV) are related to shallow and deep traps in the rubrene.

The relative intensity of the shoulder peak in the EL spectrum increases due to trap states existing in the shallow traps of the rubrene EML. Thus, the device V with a rubrene EML is attributed to increases in the width of the recombination region and in the probability of trapping charge, and the variation in the shoulder peak for the normalized EL spectrum with a rubrene EML is related to the position of the recombination region to the number of generated excitons.

Conclusions

The electrical and the optical properties of OLEDs fabricated utilizing a rubrene EML were investigated to clarify the effects of their charge balance on the carrier trapping mechanisms. The device performance of the OLEDs with a rubrene EML was optimized by changing the thicknesses of the NPB HTL and the Alq_3 ETL. The efficiency of the OLEDs was enhanced with increasing thickness of the rubrene EML. The charge trapping and the luminance mechanisms were affected by the thickness of the rubrene layer, regardless of the existence of the barrier layers. The effects of charge balance on the carrier trapping mechanisms of OLEDs with a rubrene EML were described on the basis of the current density-voltage, luminance-voltage, and EL spectra results. These results can help to improve understanding effects of charge balance on the carrier trapping mechanisms of OLEDs with a rubrene EML

Acknowledgment

This research was supported by Basic Science Research Program through the National Research Foundation of Korea (NRF) funded by the Ministry of Education, Science and Technology (2013-016467).

References

[1] Reineke, S., Lindner, F., Schwartz, G., Seidler, N., Walzer, K., Lüssem, B., & Leo, K. (2009). *Nature*, *459*, 234.
[2] Sasabe, H., Toyota, N., Nakanishi, H., Ishizaka, T., & Pu, Y. J. (2012). *Kido, J. Adv. Mater.*, *24*, 3212.
[3] Tavasli, M., Moore, T. N., Zheng, Y., Bryce, M. R., Fox, M. A., Giffiths, G. C., Jankus, V., Al-Attar, H. A., & Monkman, A. P. (2012). *J. Mater. Chem.*, *22*, 6419.
[4] Liao, L. S., Klubek, K. P., & Tang, C. W. (2004). *Appl. Phys. Lett.*, *84*, 167.
[5] Chen, Y., Chen, J., Ma, D., Yan, D., & Wang, L. (2011). *J. Appl. Phys.*, *110*, 074504.
[6] Guo, F., & Ma, D. (2005). *Appl. Phys. Lett.*, *87*, 173510.
[7] Guo, T. F., Wen, T. C., Huang, Y. S., Lin, M. W., Tsou, C. C., & Chung, C. T. (2009). *Opt. Express*, *17*, 21205.
[8] Liu, S. W., Divayana, Y., Sun, X. W., Wang, Y., Leck, K. S., & Demir, H. V. (2011). *Opt. Express*, *19*, 4513.
[9] Chang, C. C., Chen, J. F., Hwang, S. W., & Chen, C. H. (2005). *Appl. Phys. Lett.*, *87*, 253501.
[10] Zhang, H. Z., Dai, Y., Ma, D., & Zhang, H. (2007). *Appl. Phys. Lett.*, *91*, 123504.
[11] Schmidt, T. D., Buchschuster, A., Holm, M., Nowy, S., Weber, J. A., & Brutting, W. (2011). *Synth. Met.*, *161*, 637.

[12] Chen, S., Deng, L., Xie, J., Peng, L., Xie, L., Fan, Q., & Huang, W. (2010). *Adv. Mater.*, *22*, 5227.
[13] Reineke, S., Lindner, F., Schwartz, G., Seidler, N., Walzer, K., Lussem, B., & Leo, K. (2009). *Nature*, *459*, 234.
[14] Kim, K. S., Jeon, Y. M., Kim, J. M., Lee, C. W., Gong, M. S. (2008). *Org. Electron.*, *9*, 797.
[15] Fan, C. H., Sun, P., Su, T. H., & Cheng, C. H. (2011). *Adv. Mater.*, *23*, 2981.
[16] Da Silva Filho, D. A., Kim, E.-G., & Brédas, J.-L. (2005). *Adv. Mater.*, *17*, 1076.
[17] Tsuboi, T., Kishimoto, T., Wako, K., Matsuda, K., & Iguchi, H. (2012). *J. Nanosci. Nanotechnol.*, *12*, 3692.
[18] Thomschke, M., Hofmann, S., Olthof, S., Anderson, M., Kleemann, H., Schober, M., BLüssem, B., & Karl Leo. (2011). *Appl. Phys. Lett.*, *98*, 083304.